Journal of Circuits, Systems, and Computers

RANK ONE CHAOS IN SWITCH-CONTROLLED PIECEWISE LINEAR CHUA'S CIRCUIT

QIUDONG WANG*
Department of Mathematics, University of Arizona
Tucson, Arizona 85721, USA
dwang@math.arizona.edu

ALI OKSASOGLU†
Honeywell
Tucson, Arizona 85737, USA
ali.oksasoglu@honeywell.com

Received (Day Month Year)
Revised (Day Month Year)
Accepted (Day Month Year)

In this paper, we continue our study of rank one chaos in switch-controlled circuits. Periodically controlled switches are added to Chua's original, *piecewise linear* circuit to generate rank one attractors in the vicinity of an asymptotically stable periodic solution that is relatively large in size. Our previous investigations relied heavily on the smooth nonlinearity of the unforced systems, and were by large restricted to a small neighborhood of supercritical Hopf bifurcations. Whereas the system studied in this paper is much more feasible for physical implementation, and thus the corresponding rank one chaos is much easier to detect in practice. Results of PSPICE simulations are also presented.

Keywords: Rank one chaos; strange attractors; switch-controlled circuit; Chua's circuit.

1. Introduction

In this paper, we continue our study on switch-controlled circuits within the context of the theory of rank one attractors.[1,2] Switches controlled by periodic pulses are added to the original Chua's circuit[3] to generate *rank one chaos* around certain stable periodic solutions. The term "rank one chaos", as is used in this paper, indicates a number of precisely defined dynamical properties that together imply *sustained*, *observable chaos*.[4,5] These properties include (a) positive Lyapunov exponents starting from almost all initial conditions in the basin; and (b) cohesive statistical properties represented by the existence of SRB measures.

*This research is partially supported by a grant from NSF
†Also with the Department of Mathematics, University of Arizona, Tucson, Arizona 85721 USA

The development of the theory of rank one attractors has a long and celebrated history. It originated from Jakobson's theory on quadratic maps[6] and Benedicks-Carleson's theory on Hénon maps.[7,8] The main result of this theory can be stated as follows: for a given one parameter family f_a, $a \in I$ of rank one maps, i.e., maps with one direction of instability represented by 1D functions with critical points, there is a set $\Delta \subset I$ of positive measure, such that $f_a, a \in \Delta$ admits homoclinc tangles without attracting periodic orbits (sinks)[1,2] (for a brief exposition of this theory, also see Ref. [5]). One important objective that this new mathematical theory fulfils is that it provides a rigorous mathematical justification for pictures of chaos generated in simulations. Using the theory, homoclinic tangles with one direction of instability (rank one) represented by non-uniformly hyperbolic 1D maps can be carefully analyzed, and the exceedingly complicated geometric and dynamical structures of these tangles can be fully understood in comprehensive mathematical terms.

In Refs. [4, 9], the authors proposed a systematic way of generating rank one chaos in applications. To start let us take a system

$$\frac{d\mathbf{u}}{dt} = f(\mathbf{u}) \tag{1}$$

and assume that Eq. (1) has an asymptotically stable periodic solution. To create rank one chaos, we add a time periodic forcing term to Eq. (1) to obtain

$$\frac{d\mathbf{u}}{dt} = f(\mathbf{u}) + \varepsilon\Phi(\mathbf{u})P_T(t) \tag{2}$$

where $P_T(t)$ is a periodic pulse train of period T. It was proved in Ref. [9] that, for any given periodic solutions of Eq. (1) that is asymptotically stable, there exists proper choices of $\Phi(\mathbf{u})$, such that Eq. (2) admits rank one chaos in the vicinity of that periodic solution. To be more precise,

Theorem 1. (Creation of rank one attractors from arbitrary limit cycles) Let φ_t be a C^4 flow[a] in $\mathbb{R}^n$, and assume that φ_t has an asymptotically stable periodic solution γ. Let U be a neighborhood of γ, and let $\mathrm{Emb}^3(U, \mathbf{R}^n)$ be the space of C^3 embeddings of U into $\mathbb{R}^n$. Then there is an open set $\mathcal{E} \subset \mathrm{Emb}^3(U, \mathbb{R}^n)$ such that, for every $\kappa \in \mathcal{E}$, [b] $\varphi_T \circ \kappa$ has a rank one attractor for a positive measure set of T.

This theorem is a special version of theorem 1 proved in Ref. [9]. In concrete applications, stable periodic solutions are easy to find but the options for the actual implementations of the forcing terms are usually restricting. Within the general framework of Ref. [9], it is not likely that the proposed forms of forcing used in the proof of the theorem stated above, represented by $\Phi(\mathbf{u})$ in Eq. (2), are feasible in terms of physical implementation. There is, however, one situation where the practical concerns on $\Phi(\mathbf{u})$ can be effectively diminished. This is the case when the

[a] Defined, say, by the unforced system of Eq. (1)
[b] Each of which corresponding to a special design of the forcing term in Eq. (2)

stable limit cycle we use is freshly coming out of the center of a supercritical Hopf bifurcation. In this case the conditions on $\Phi(\mathbf{u})$ is much less restrictive and the creation of rank one attractors relies more on the normal forms of the unforced system than the form of $\Phi(\mathbf{u})$. Actually, in the case of Hopf limit cycles, it is possible to give an explicit, recipe-like procedure to create strange attractors.[10]

The theory of Ref. [9] is first applied to the Chua's circuit in Ref. [5], then to the MLC (Murali-Lakshmanan-Chua) circuit[11] in Ref. [12]. Both theoretical justifications and numerical simulations are presented to confirm the validity of the scheme proposed in Ref. [9] in creating rank one chaos in the vicinity of the supercritical Hopf bifurcations of the original circuits. Later, switches controlled by periodic pulses are introduced[10] to represent the forcing terms of Eq. (2). The effects of different switch control schemes are also investigated, and the results of our numerical simulations are in perfect match with the theoretical predictions of Ref. [9] in the scenario of Hopf bifurcations.

In order to have a generic supercritical Hopf bifurcation, however, local nonlinearity is a necessity. For instance, in our previous study[10] of the Chua's circuit, a cubic nonlinearity for the nonlinear resistor characteristics replaced the original piecewise linear design that is much easier to implement in practice. Moreover, having to be restricted to a small neighborhood of some tiny Hopf limit cycle may also be seen as a potential drawback in terms of practical implementations and detections of rank one attractors.

In this paper, we use the original *piecewise linear* Chua's circuit, and impose again specific forcing terms by adding periodically controlled switches. These switches are turned on and off to kick limit cycles of a visible size. One of the main reasons for using the original Chua's circuit is the feasibility in circuit construction and the ease of physical detection of rank one chaos. Our numerical simulations continue to generate pictures of rank one chaos, and these results are further verified by PSPICE simulations.

2. System Under Study

The set of nondimensional equations for the original Chua's system is given by

$$\begin{aligned} \frac{dx}{dt} &= \alpha[y - h(x)] \\ \frac{dy}{dt} &= \gamma[x - y + \eta z] \\ \frac{dz}{dt} &= -\beta y \end{aligned} \tag{3}$$

where $h(x) = m_1 x + 0.5(m_0 - m_1)(|x + B_p| - |x - B_p|)$. Equation (3) is obtained from the original Chua's circuit in Fig. 1, with $f(v_1) = G_b v_1 + 0.5(G_a - G_b)(|v_1 + V_b| - |v_1 - V_b|)$, through the following change of variables:

$$x = v_1/V_0 \qquad y = v_2/V_0 \qquad z = i/I_0 \qquad t \to t/\omega_n \tag{4}$$

where V_0, I_0, and ω_n are the arbitrary voltage, current, and frequency scaling constants, respectively. In this case, in terms of the physical system parameters, the nondimensional system parameters in Eq. (3) are given by

$$\begin{aligned} \alpha = \frac{G}{C_1\omega_n},\ \gamma = \frac{G}{C_2\omega_n},\ \eta = \frac{RI_0}{V_0},\ \beta = \frac{V_0}{L\omega_n I_0} \\ m_0 = \frac{G_a}{G},\ m_1 = 1 + \frac{G_b}{G},\ B_p = \frac{V_b}{V_0} \end{aligned} \tag{5}$$

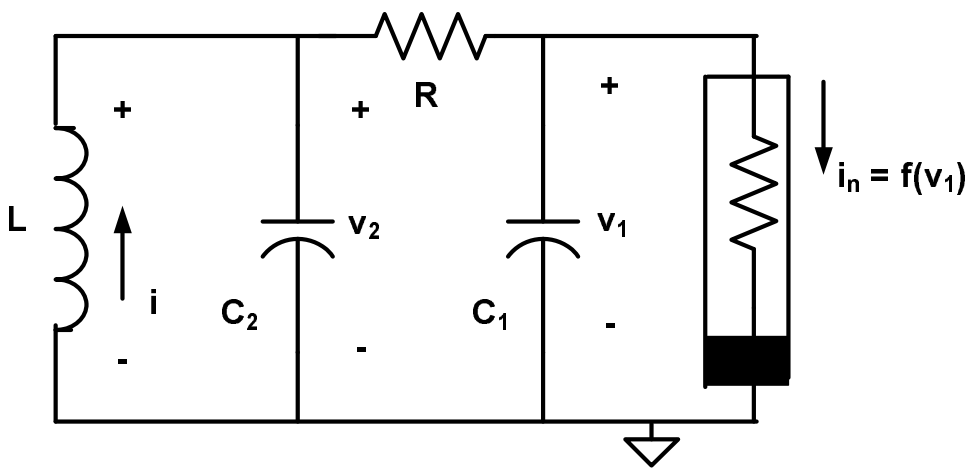

Fig. 1. Original Chua's circuit.

The circuit studied in this paper is depicted in Fig. 2. Each switch added is controlled by an external periodic pulse train with a pulse width of p_0 and a period of T_0. When all the switches in Fig. 2 are kept open or at their default positions, we have the original Chua's circuit. The nondimensional set of equations for the circuit of Fig. 2 can be given by

$$\begin{aligned} \frac{dx}{dt} =& \alpha[y - h(x)] - \varepsilon_1 x P_{p,T}(t) \\ \frac{dy}{dt} =& \gamma[x - y + \eta z] - \varepsilon_2 y P_{p,T}(t) \\ \frac{dz}{dt} =& -\beta y - \varepsilon_3 z P_{p,T}(t) \end{aligned} \tag{6}$$

The relationship between the new parameters of the nondimensional system of Eq.

(6) and those of the physical circuit of Fig. 2 can be given by

$$\begin{aligned} p &= p_0\omega_n, \quad T = T_0\omega_n \\ P_{p,T} &= \frac{1}{p}\sum_{n=0}^{\infty}[u(t-nT) - u(t-nT-p)] \\ \varepsilon_1 &= \frac{\alpha R p}{R_1}, \quad \varepsilon_2 = \frac{Rp}{R_2}, \quad \varepsilon_3 = \frac{\eta\beta R_3 p}{R} \end{aligned} \tag{7}$$

where $P_{p,T}(t)$ is a periodic pulse train with a pulse width of p and a period of T, and ε_i represent the magnitudes of these periodic pulse trains. Equation (6) is in the form of Eq. (2).

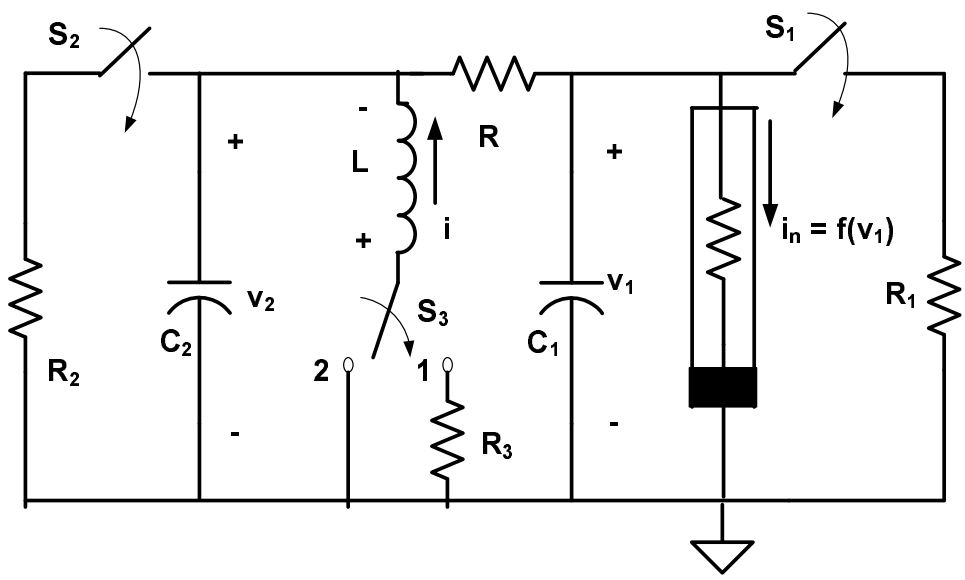

Fig. 2. Switch-controlled Chua's circuit.

The autonomous part of (6), obtained by setting $\varepsilon_1 = \varepsilon_2 = \varepsilon_3 = 0$, has a limit cycle, as shown in Fig. 3, for

$$(\alpha, \gamma, \beta, \eta, m_0, m_1, B_p) = (2.0, 1.0, 2.0, 1.12, -0.75, -0.225, 1.0) \tag{8}$$

This limit cycle is the one that is going to be forced to obtain rank one chaos.

3. Results of Simulations

3.1. *Numerical Simulations*

In this subsection, we present the results of our numerical simulations. Computations are performed using the fourth-order Runge-Kutta routine starting at $t_0 = 0$.

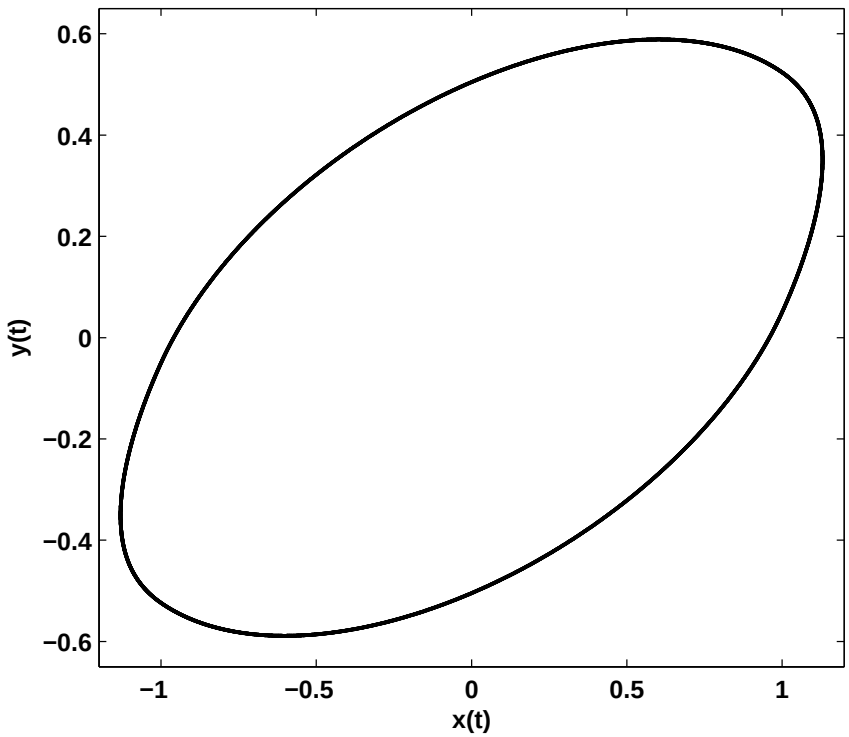

Fig. 3. A non-Hopf limit cycle.

For all pictures presented, one discrete orbit started near the attractor for the time-T map is presented. We let

$$\alpha = 2,\ \gamma = 1, \eta = 1.12,\ m_0 = -0.75,\ m_1 = 0.225,\ B_p = 1 \tag{9}$$

be fixed throughout and only allow T and ε_i to vary. With the choices of the values of Eq. (9), we obtain the limit cycle shown in Fig. 3 by letting $\varepsilon_1 = \varepsilon_2 = \varepsilon_3 = 0$.

Figures 4-6 are examples of rank one chaos. For these simulations we set $\varepsilon_2 = \varepsilon_3 = 0$ so there is only one switch ($\mathbf{S_1}$ in Fig. 2) in action.

Although the attractor in Fig. 4 appears to be a simple closed curve, it is in fact a chaotic attractor of very complicated geometrical and dynamical structure. This is reflected in the middle ($x(kT)$ versus kT) and bottom (Fourier spectrum of $x(kT)$) portions of Fig. 4. The middle portion of Fig. 4 shows a complete random evolution of the x coordinate versus time, and the bottom portion a continuous Fourier spectrum. With a very large forcing period ($T = 251$), the geometric structure in the radial direction is compressed towards the limit circle of Fig. 3. To reveal more of the structure in the radial direction, we reduce the value of T to 71.5 in Fig.

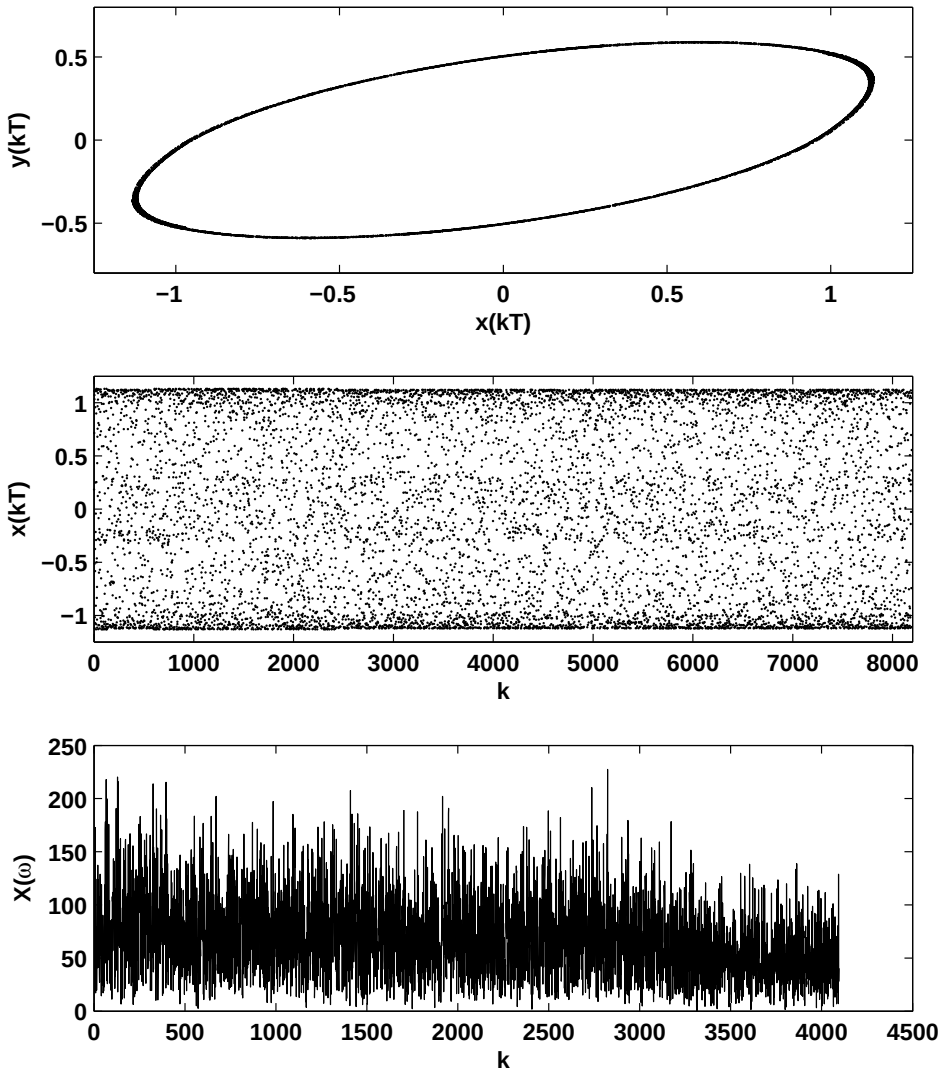

Fig. 4. Strange attractor, $T = 251.0, \varepsilon_1 = 0.5, \varepsilon_2 = \varepsilon_3 = 0$. Time-T map (top), $x(kT)$ versus kT (middle), frequency spectrum of $x(kT)$ (bottom).

5, and a nice fractal structure starts to show up. In Fig. 6, we further reduce the value of T to 35.5 and set $\varepsilon_1 = 0.99$. The chaotic attractor of Fig. 6 does not appear

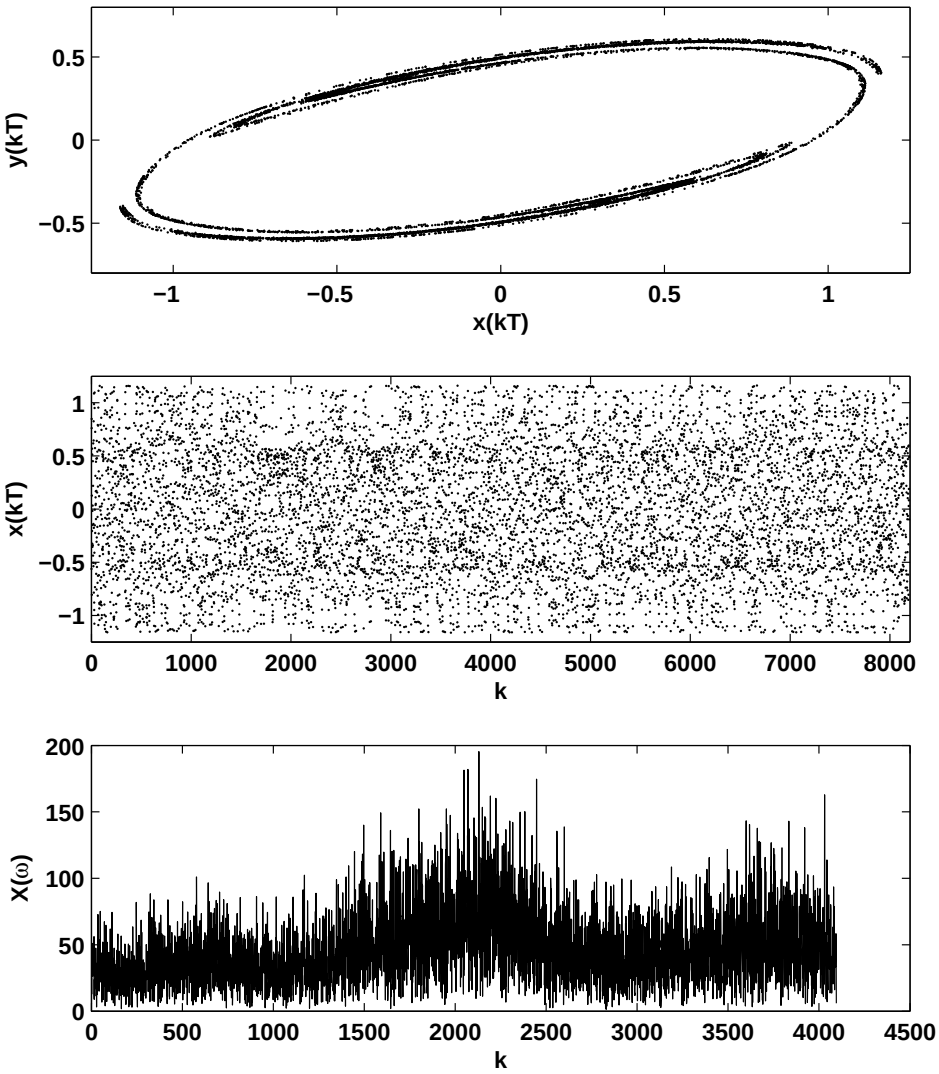

Fig. 5. Strange attractor, $T = 71.5, \varepsilon_1 = 0.5, \varepsilon_2 = \varepsilon_3 = 0$. Time-T map (top), $x(kT)$ versus kT (middle), frequency spectrum of $x(kT)$ (bottom).

as smooth in shape as the ones we obtained in our previous studies.[5,10,12] This is due to the fact that we are working here with a piecewise linear system that is

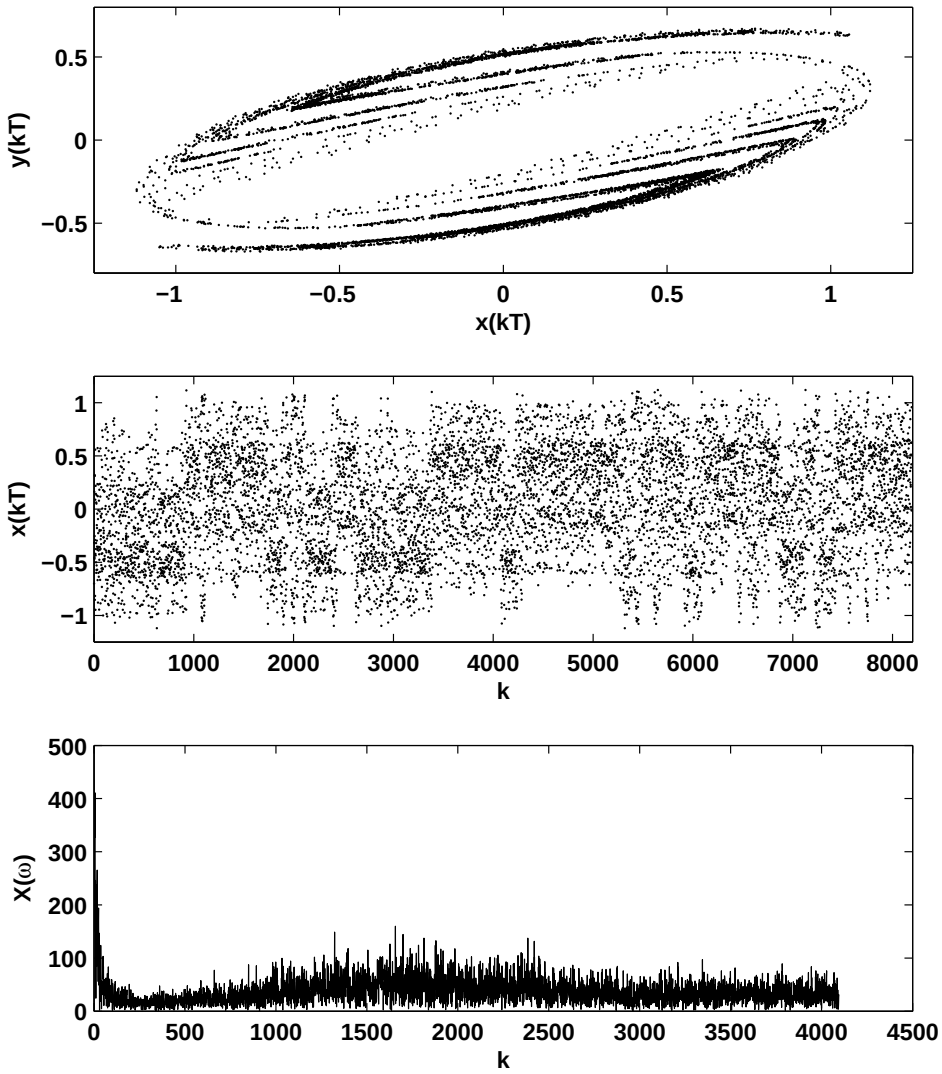

Fig. 6. Strange attractor, $T = 35.5, \varepsilon_1 = 0.99, \varepsilon_2 = \varepsilon_3 = 0$. Time-T map (top), $x(kT)$ versus kT (middle), frequency spectrum of $x(kT)$ (bottom).

intrinsically not smooth. Our simulations again exhibit sensitive dependence of the strange attractors on the values of parameters. For instance, by adjusting the value

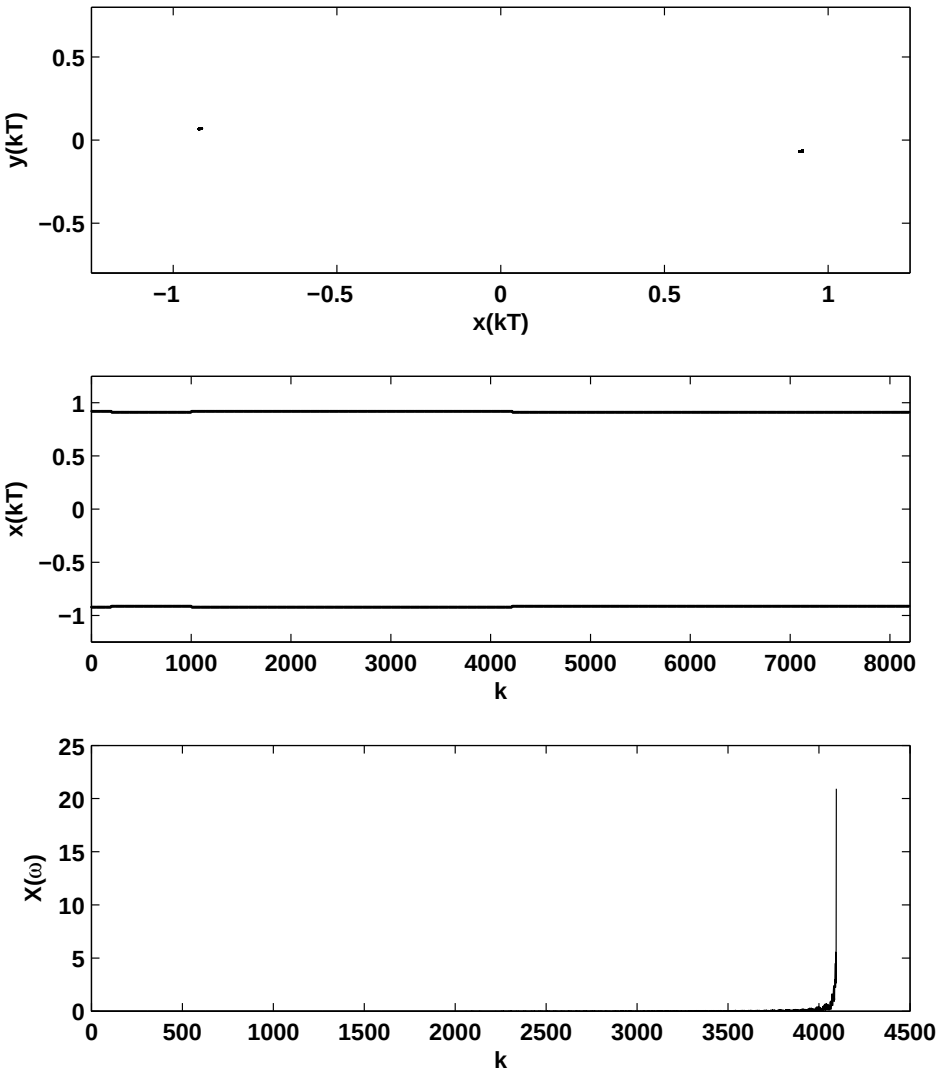

Fig. 7. Periodic sink, $T = 72.0, \varepsilon_1 = 0.5, \varepsilon_2 = \varepsilon_3 = 0$. Time-T map (top), $x(kT)$ versus kT (middle), frequency spectrum of $x(kT)$ (bottom).

of T from 71.5 in Fig. 5 to 72, the picture changes from that of a chaotic attractor to that of a periodic sink as shown in Fig. 7. This is completely in line with the

predictions of the theory of rank maps: that is, the parameters of observable chaos form a set of positive measure that is nowhere dense, and the scenarios of periodic sinks and observable chaos are the two main competing dynamical scenarios.

In Figs. 8 and 9 we put other switches of Fig. 2 in action. For Fig. 8, $\varepsilon_1 = 0.36, \varepsilon_2 = 0.17, \varepsilon_3 = 0$ and $T = 72.0$. For Fig. 9, $\varepsilon_1 = 0.36, \varepsilon_1 = 0.1, \varepsilon_3 = 0.1$ and $T = 87.5$.

Remarks: (1) According to Theorem 1, any given asymptotically stable periodic solution can be appropriately kicked into forming a chaotic rank one attractor. However, the forcing used in the proof of this theorem is fairly restrictive and, for most applications, is not feasible for physical implementations.

(2) The studies of this paper are based on a forcing that is created by adding periodically controlled switches to autonomous circuits with asymptotically stable oscillations. This specific form of forcing is, in general, different from the one used in the proof of Theorem 1. For this specific design, there is no theoretical assurance that rank one chaos would arise. We know, however, that they are more likely to occur if the periodic solution is weakly stable, and the *shearing* around this solution is relatively strong. The *shearing* here means that the points at different distances from the center of the limit cycle rotate at different speeds, thus it has the effect of amplifying the initial deformation caused by the external forcing. In the case of a supercritical Hopf bifurcation, the stability of the Hopf limit cycle can be made as weak as desired and the strength of shearing can be analytically computed.[5] Hence, the parameters of strong shearing are easily identified. This led to the investigations of Refs. [5, 10, 12], where a systematic way of finding the locations of rank one chaos in switch-controlled systems was presented. For a stable periodic solution arbitrarily picked, however, finding weakly stable limit cycles with strong shearing through analytical computations is usually not a realistic option. In this case we have to rely more on trial and error in simulations.

(3) Let us now point out a main difference between the creation of rank one attractors in this paper and in the ones in Refs. [5, 10, 12]. Previously, we had focused on the surroundings of a supercritical Hopf bifurcation for which strong shearing is ensued by the local nonlinearity of the unforced system. For the *piecewise linear* system of Eq. (1) studied in this paper, however, there is no local nonlinearity therefore no Hopf bifurcations. The phase space is, in fact, divided into three regions where the original circuit is defined by three different linear equations. When restricted completely to one of the linear regions, shearing is obviously non-existent so the ultimate reason for the creation of rank one chaos is the jumps of a solution from one region of linearity to another. The lack of smoothness that, for example, appears in Fig. 7 is a reflection of these sudden jumps.

(4) Other aspects worth emphasizing here are that (a) the chaos seen in our simulations is exactly the type of chaos the theory predicts, and (b) the *observability* of these chaotic attractors stems from the fact that they result from homoclinic tangles without attracting periodic sinks.

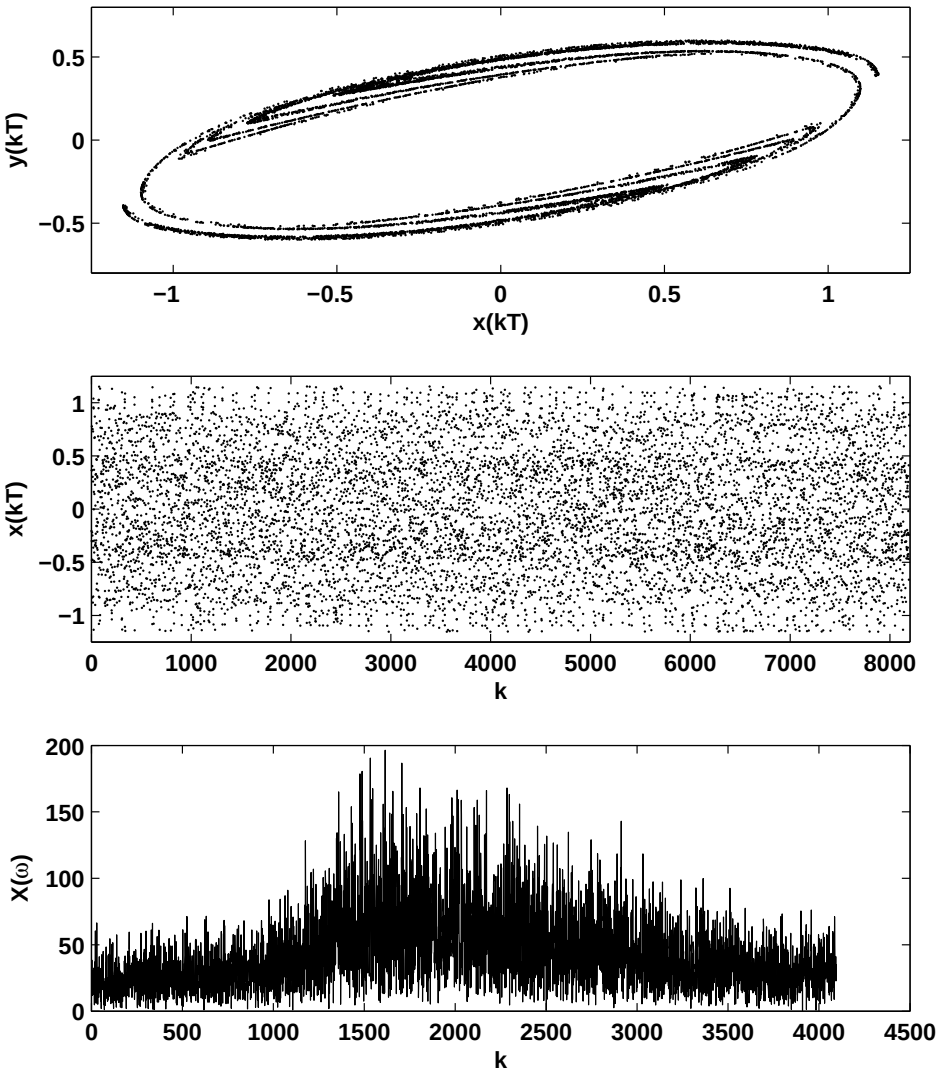

Fig. 8. Strange attractor, $T = 72.0, \varepsilon_1 = 0.36, \varepsilon_2 = 0.17, \varepsilon_3 = 0$. Time-T map (top), $x(kT)$ versus kT (middle), frequency spectrum of $x(kT)$ (bottom).

3.2. *PSPICE Simulations*

In this subsection, we present the results of the PSPICE simulations for the parameters of Figs. 4-9. That is, the parameter values used in PSPICE simulations

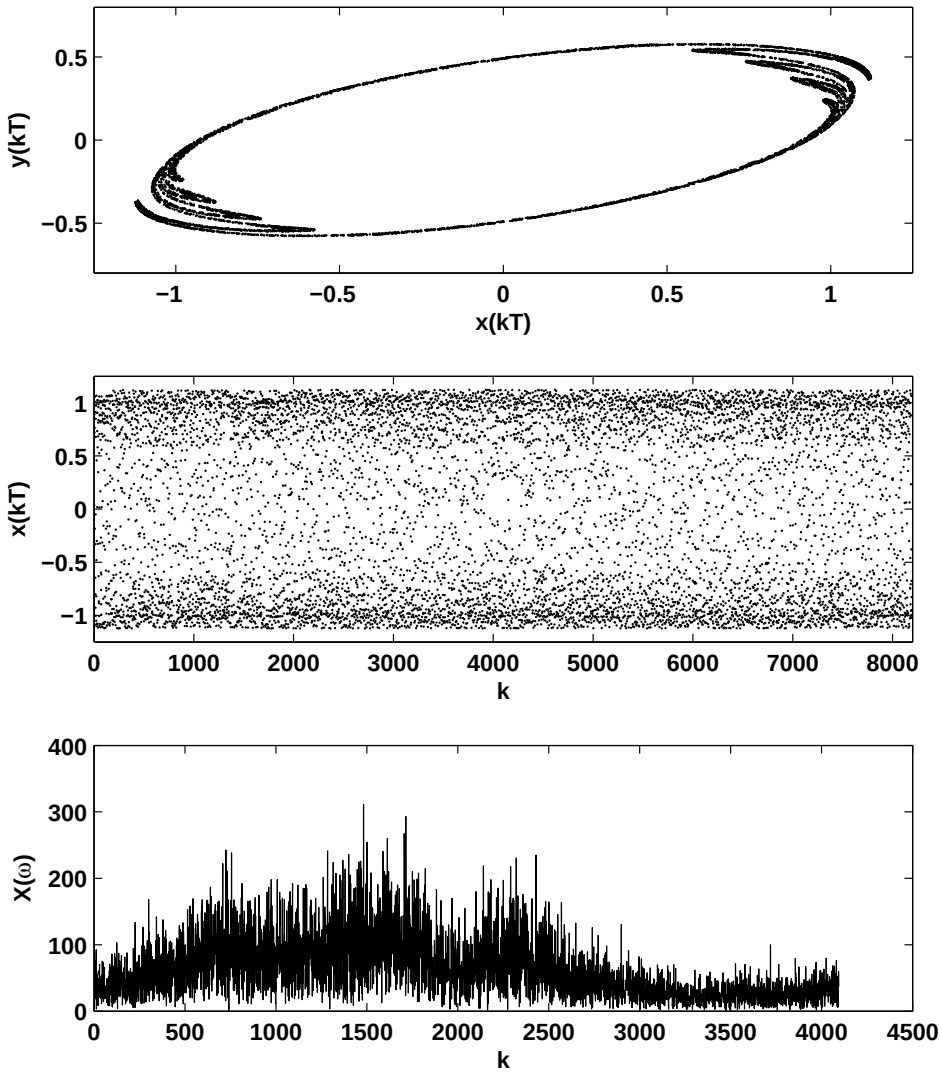

Fig. 9. Strange attractor, $T = 87.5, \varepsilon_1 = 0.36, \varepsilon_2 = 0.1, \varepsilon_3 = 0.1$. Time-T map (top), $x(kT)$ versus kT (middle), frequency spectrum of $x(kT)$ (bottom).

for Figs. 10-15 are the same as those used in numerical simulations for Figs. 4-9, respectively. Our simulation results suggest a close match between the PSPICE and

purely numerical simulations.

4. Conclusion

In this paper, we have demonstrated how to create rank one chaos from arbitrary limit cycles using the theory developed in Refs. [1, 2]. For that purpose, switches controlled by periodic pulse trains are added to the Chua's original *piecewise linear* circuit to generate rank one attractors in the vicinity of an asymptotically stable periodic solution that is relatively large in size. The previous investigations conducted in Refs. [5, 10, 12] relied heavily on the nonlinearity of the unforced systems, and were, by large, restricted to a small neighborhood of supercritical Hopf bifurcations. Whereas, the system studied in this paper is much more feasible for physical implementation, and the corresponding rank one chaos is much easier to detect. The results of our numerical computations and PSPICE simulations presented in this paper confirm the existence of rank one chaos in the system studied.

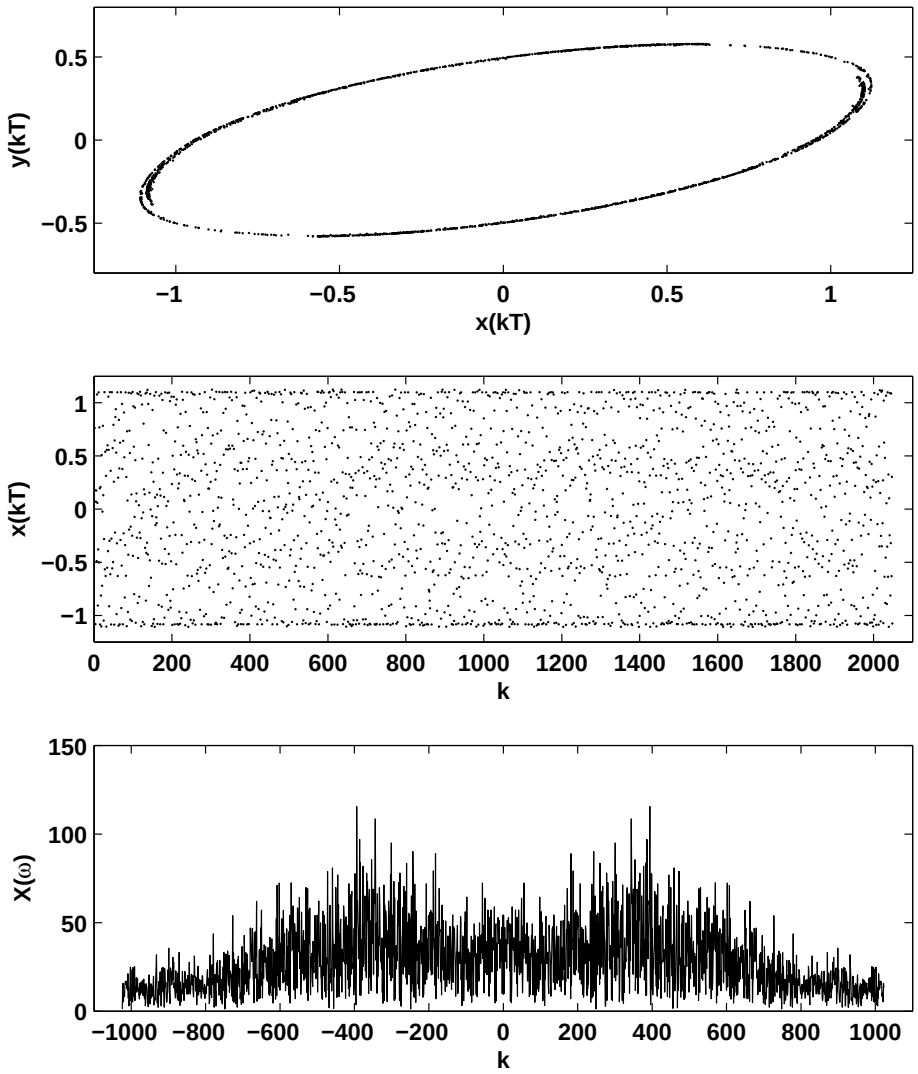

Fig. 10. Corresponding PSPICE simulations for Fig. 4. Time-T map (top), $x(kT)$ versus kT (middle), frequency spectrum of $x(kT)$ (bottom).

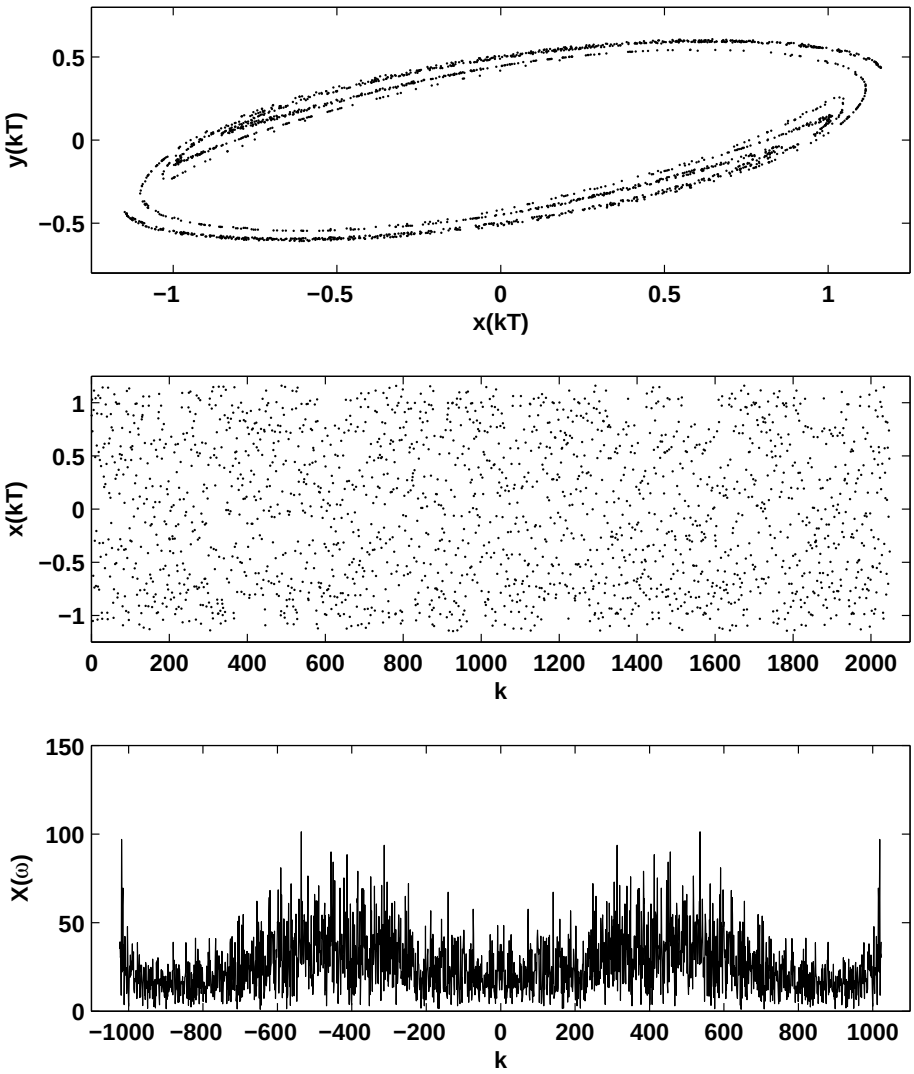

Fig. 11. Corresponding PSPICE simulations for Fig. 5. Time-T map (top), $x(kT)$ versus kT (middle), frequency spectrum of $x(kT)$ (bottom).

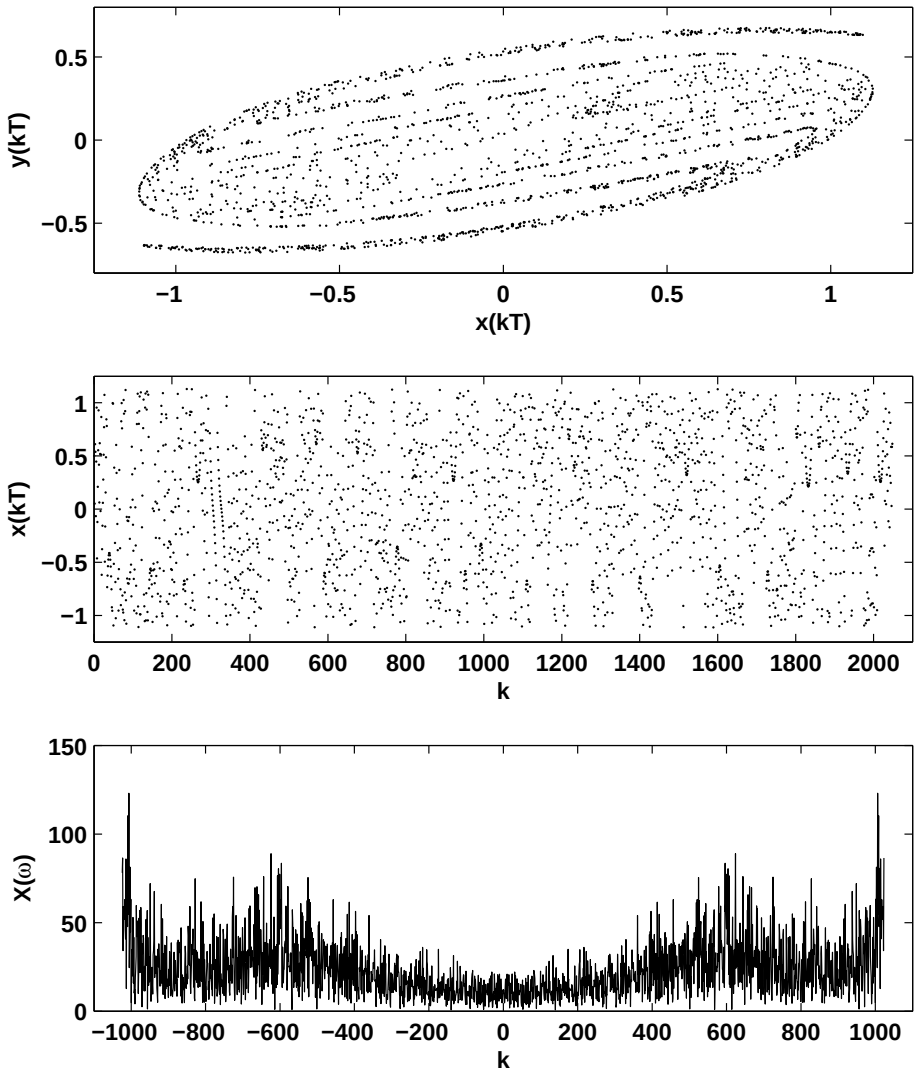

Fig. 12. Corresponding PSPICE simulations for Fig. 6. Time-T map (top), $x(kT)$ versus kT (middle), frequency spectrum of $x(kT)$ (bottom).

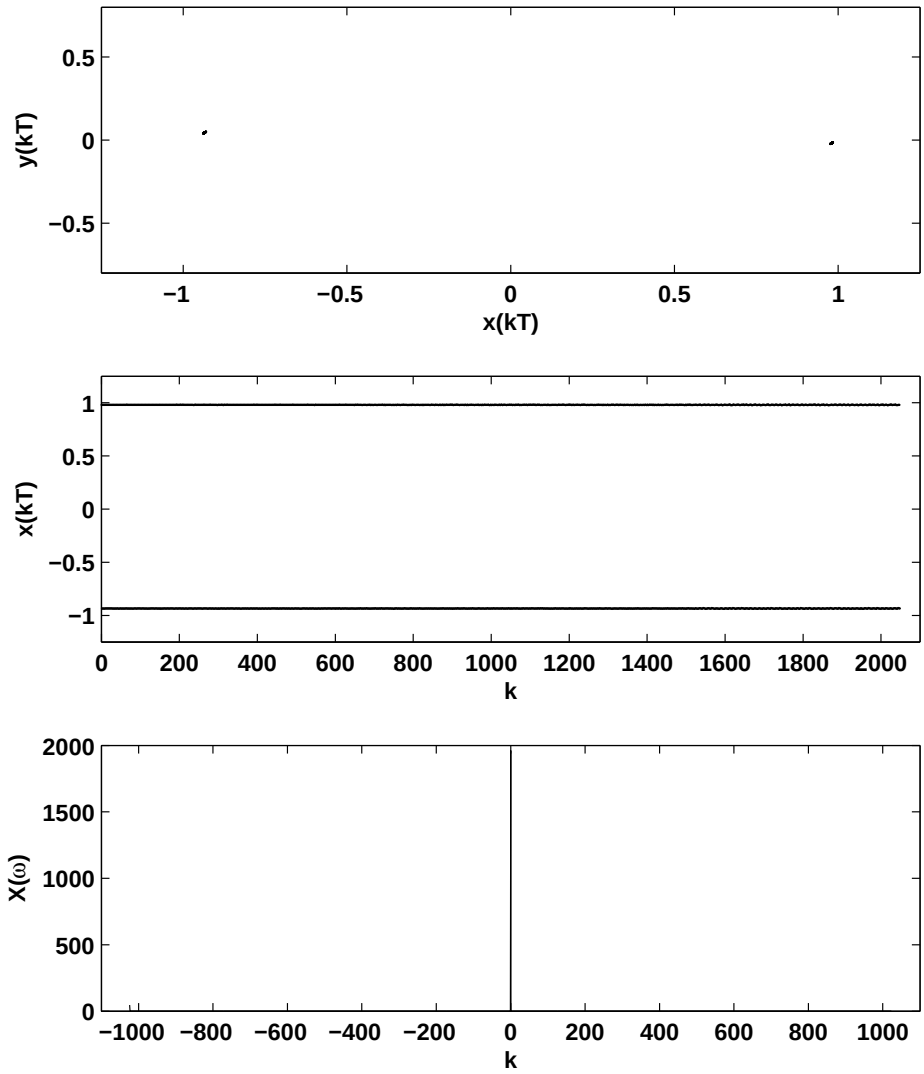

Fig. 13. Corresponding PSPICE simulations for Fig. 7. Time-T map (top), $x(kT)$ versus kT (middle), frequency spectrum of $x(kT)$ (bottom).

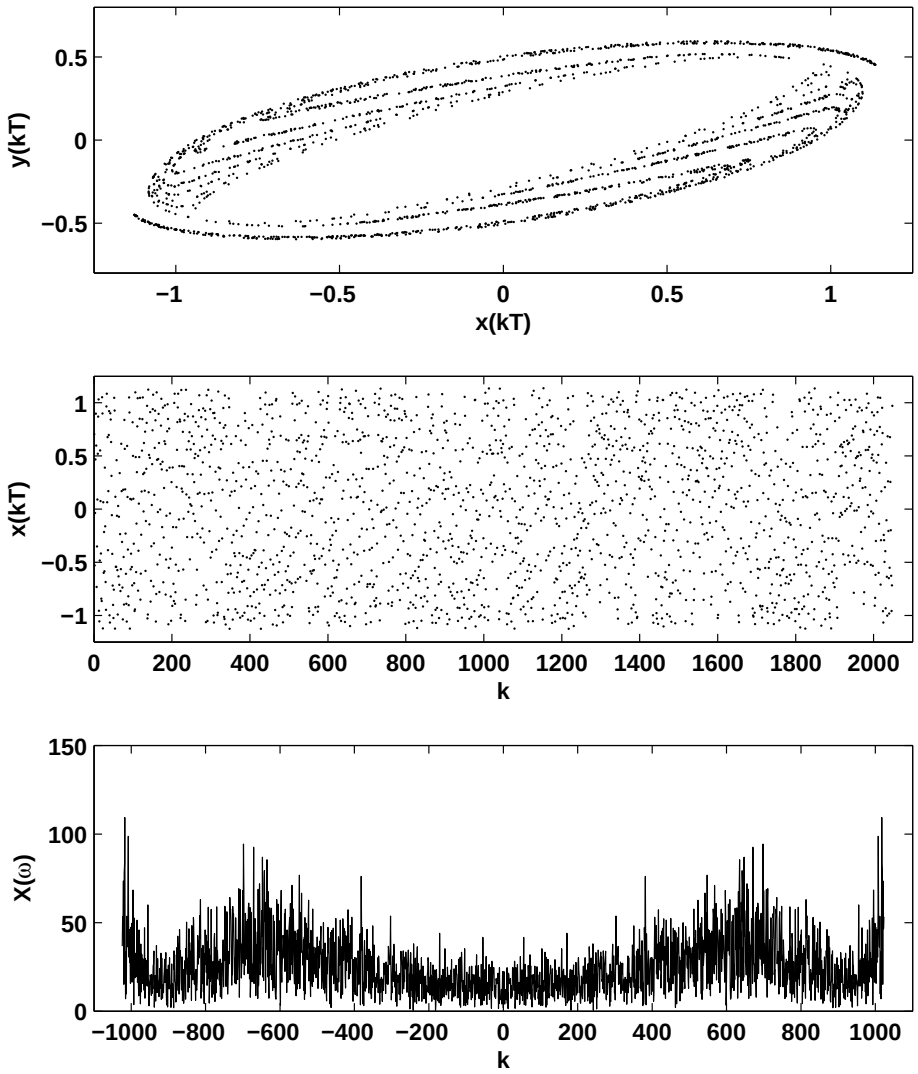

Fig. 14. Corresponding PSPICE simulations for Fig. 8. Time-T map (top), $x(kT)$ versus kT (middle), frequency spectrum of $x(kT)$ (bottom).

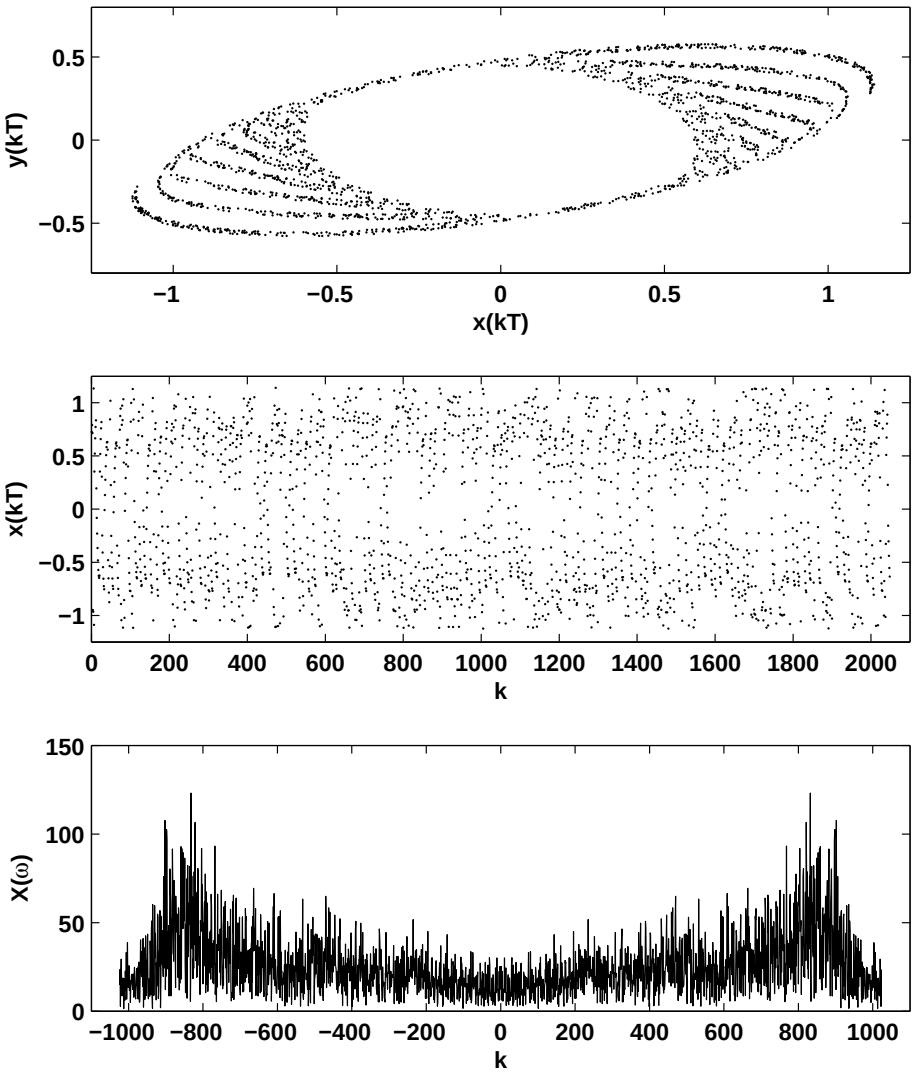

Fig. 15. Corresponding PSPICE simulations for Fig. 9. Time-T map (top), $x(kT)$ versus kT (middle), frequency spectrum of $x(kT)$ (bottom).

References

1. Q. Wang, L.-S. Young, Strange attractors with one direction of instability, *Commun. Math. Phys.* **218** (2001) 1–97.
2. Q. Wang, L.-S. Young, Toward a theory of rank-one attractors, *In preprint.*
3. L. O. Chua, Chua's circuit. An overview ten years later, *J. Circuits Syst. Comput.* **4** (1994) 117–159.
4. Q. Wang, L.-S. Young, From invariant curves to strange attractors, *Commun. Math. Phys.* **225** (2002) 275–304.
5. Q. Wang, A. Oksasoglu, Strange attractors in periodically kicked Chua's circuit, *Int. J. Bifurc. Chaos.* **16** (2005) 83–98.
6. M. Jakobson, Absolutely continues invariant measures for one-parameter families of one-dimensional maps, *Commun. Math. Phys.* **81** (1981) 39–88.
7. M. Benedicks, L. Carleson, On iterations of $1-ax^2$ on $(-1,1)$, *Ann. Math.* **122** (1985) 1–25.
8. M. Benedicks, L. Carleson, The dynamics of the Hénon map, *Ann. Math.* **133** (1991) 73–169.
9. Q. Wang, L.-S. Young, Strange attractors in periodically-kicked limit cycles and Hopf bifurcations, *Commun. Math. Phys.* **240** (2002) 509–529.
10. A. Oksasoglu, D. Ma, Q. Wang, Rank one chaos in a second-order switch-controlled circuit, To be published in *Int. J. Bifurc. Chaos.* (2006)
11. K. Murali, M. Lakshmanan, L. O. Chua, The simplest dissipative nonautonomous chaotic circuit, *IEEE Trans. Circuits Syst. I* **41** (1994) 462–463.
12. A. Oksasoglu, Q. Wang, Hopf bifurcations and chaos in a second-order system, To be published in *Int. J. Bifurc. Chaos.* (2006)